Ablation of ATJ Graphite at High Temperatures

JOHN H. LUNDELL* AND ROBERT R. DICKEY†
NASA Ames Research Center, Moffett Field, Calif.

Results of an extensive experimental program on the ablation of ATJ graphite in air at surface pressures of 0.3 to 4.4 atm and surface temperatures of 2570 to 4030°K are presented. The measured mass-loss rates are correlated with surface temperature, pressure, and effective nose radius. The results are compared with several equilibrium thermochemical ablation theories which differ basically in the chemical species that are considered and in the thermodynamic properties assigned to these species. All the theories predict about the same mass-loss rate in the diffusion-controlled oxidation regime and are in good agreement with the experimental results. At higher temperatures, however, the experimental and theoretical results do not agree. At temperatures above 3700°K, the experimental mass-loss rate becomes independent of pressure and an exponential function of temperature. A comparison of the high-temperature results with the theories indicates that all the theories, except the one based on the thermodynamic properties from the JANAF tables, are invalid because they overpredict the mass-loss rate. On the other hand, the theory based on the JANAF properties underpredicts the measured mass-loss rate by a factor of three at 4000°K. At least a portion of this difference between experiment and theory is attributed to particulate mass loss which is visually observed.

Nomenclature

B' = nondimensional mass-loss parameter
C_H = Stanton number in the presence of blowing
C_{H_0} = Stanton number in the absence of blowing
$\dot{m}_d$ = mass-loss rate in the diffusion-controlled oxidation regime, g/cm^2 sec
$\dot{m}_e$ = experimental mass-loss rate, g/cm^2 sec
$\dot{m}_t$ = theoretical thermochemical mass-loss rate, g/cm^2 sec
$\Delta\dot{m}$ = incremental mass-loss rate, g/cm^2 sec
p_s = surface pressure, atm
q_c = cold-wall convective heating rate, w/cm^2
R_{n_e} = effective nose radius, cm
R_{n_f} = final nose radius, cm
R_{n_i} = initial nose radius, cm
T_s = surface temperature, °K
V_s = surface recession rate, cm/sec

Introduction

GRAPHITIC materials offer great potential as ablative materials for both planetary entry probe and ballistic missile applications. Entry probes into the atmospheres of the large outer planets will encounter extremely high combined radiative and convective heating rates and moderately high surface pressures. For example, Tauber and Wakefield[1] have calculated that a Jovian entry probe may sustain net heating rates to the surface of 5 to 100 kw/cm^2 and surface pressures to 30 atm, depending upon the entry conditions, atmospheric composition, and entry body weight and configuration. On the other hand, missiles with high ballistic coefficients encounter very high convective heating rates, surface pressures, pressure gradients, and aerodynamic shear stresses. For both these severe heating environments, the high heat of sublimation and the excellent high-temperature properties of graphitic materials make them a prime candidate for both nose tips and heat shields.

With these properties in mind, Tauber and Wakefield also calculated the performance of graphite as a heat shield material for Jovian entry probes. These calculations indicate that the heat shield weight, exclusive of insulation and structure, will constitute about 40% of the entry body weight. Thus it is apparent that the heat shield will be a major problem in the design of a Jovian entry probe.

In order to make calculations such as those mentioned, a set of thermodynamic properties must be selected. Tauber and Wakefield used the properties given in the JANAF tables.[2] There is, however, considerable controversy in the literature regarding the validity of the early JANAF data for the species C_3 and higher molecular weight carbon species, as well as for CN. In recent years, new thermochemical ablation theories, based on different sets of species and properties, have appeared in the literature.[3-5] The effects of the different sets of species and properties on the ablation of graphite has been demonstrated by Rindal and Powars.[6] They calculated the performance of a graphite nose tip on a missile using the different sets of species and properties. For a tip radius of 1.27 cm, the stagnation point surface temperature varied from 4000° to 4780°K, and the tip recession varied from 1.78 to 3.25 cm, depending upon which set of species and properties was used. From these results, we can conclude that the species selected and the properties assigned to those species can have a marked effect on predicted thermochemical ablation performance of graphite.

One way to determine which graphite ablation theory (and corresponding sets of species and properties) is correct, is to perform high-temperature ablation tests and compare the results with the theories. At present, however, there is very little experimental data in the literature, and what data do exist[7-10] are not sufficient to validate any one of the ablation theories.‡ Thus a comprehensive experimental program was initiated to investigate the ablative behavior of graphite in the sublimation regime.

A further objective of the program was to determine if there are significant ablation mechanisms other than those accounted for in the elementary thermochemical ablation theories. For example, experimental work by Maahs and Schryer[11] indicates that there may be particulate removal due to aerodynamic erosion, but they give no indication of the magnitude of the particulate loss. Other work[4] has shown that particulate mass

Presented as Paper 71-418 at the AIAA 6th Thermophysics Conference, Tullahoma, Tenn., April 26–28, 1971; submitted April 26, 1971; revision received September 18, 1972.
Index category: Material Ablation.
* Research Scientist. Member AIAA.
† Research Scientist.

‡ Much additional work on the ablation of graphite for application to ballistic missile nose tips has been sponsored by the U.S. Air Force. Generally, this work has been done at very high surface pressures and low stream enthalpies, and the resultant surface temperatures have not been measured.

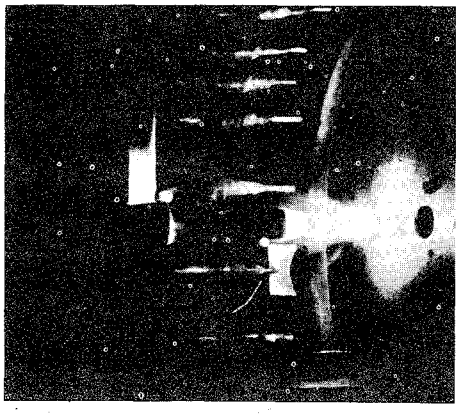

Fig. 1 Typical test in progress.

loss is very significant for ballistic missile nose tips where the pressure may exceed 100 atm. If this mechanism proves to be significant at pressures below 30 atm, the theoretical thermochemical calculations of Tauber and Wakefield[1] may underpredict the heat shield weight requirements for a Jovian entry probe.

This paper presents the results of the investigation of the high-temperature ablation of ATJ graphite in an airstream. First the facility, instrumentation, and experimental techniques are described. Then, after a brief discussion of the various ablation theories, the experimental results are presented, and the theories are assessed by comparison with the results. Finally, particulate removal is discussed.

Experiments

Facility and Instrumentation

All of the tests were performed in the Ames Heat Transfer Tunnel which is a conventional arc-driven wind tunnel. The facility is designed such that a variety of electric arc heaters and nozzles may be employed to produce a supersonic, high enthalpy, underexpanded freejet. For the present tests, a Linde model N4000 and a model N4001 arc heater were used, most of the tests being performed with the N4001 heater. By varying the length of the downstream electrode and the input power, the total enthalpy of the stream can be varied over a broad range. For these tests, electrode lengths of 28, 43, and 81 cm were used. The electric arc heaters were coupled to one of three nozzles, an 8.6 cm diam conical nozzle, a 5.5 cm diam conical nozzle, or a 5.1 cm diam contoured nozzle. All three nozzles employ a 1.9 cm diam throat, so the Mach number varied from about 3.1 to 3.8. The test chamber contains 18 support arms which are sequentially inserted into the stream by means of a stepping switch and automatic timer. With this arrangement, it is possible to obtain stream characterization data as well as ablation data during the same run, thereby eliminating uncertainty regarding arc heater repeatability. A number of the support arms, instruments, and ablation specimens are visible in Fig. 1 which is a photograph of a typical run in progress.

In general, the instrumentation inserted into the stream consists of slug-type transient calorimeters, stream survey probes, and a stream profile plate. The heating-rate profile across the stream is measured with a 1.6 cm diam water-cooled calorimeter (Hy-Cal Engineering Co.), and the pressure profile is measured with a heat sink copper pitot probe. In addition to the survey probes, a number of slug-type transient calorimeters, in a variety of sizes and shapes, are inserted into the stream. By using several different size hemispherical calorimeters, as well as flat-face and blunt calorimeters, the effective nose radius of nonhemispherical shapes can be determined experimentally. A final device inserted into the stream is a profile plate. This is simply a 0.32 cm thick stainless steel plate which quickly ablates and gives an immediate qualitative indication of the heating-rate distribution. In all cases, the instrumentation and the ablation specimens are inserted downstream of the nozzle exit at a distance equivalent to about 60% of the nozzle exit diameter. This constraint is imposed by the necessity to view the specimen surface with pyrometers at an angle of about 45°.

The number and variety of instruments inserted during a given run depends upon the severity of the heating conditions. During a typical run at moderate conditions, eight ablation specimens and ten calorimeters and other instruments are inserted. At the more severe conditions, instrumentation is restricted because survival becomes a problem. During almost all runs, however, at least a pressure survey probe, a profile plate, and one or more slug-type calorimeters were inserted.

Instrumentation external to the test chamber consists of automatic optical pyrometers and a motion picture camera. Two pyrometers are used so that the monochromatic brightness temperature can be determined at two different wavelengths. The pyrometers used are a Thermodot model TD-9 (Infrared Industries, Inc.) which has a bandpass at 0.8 μ and a Pyro 650 (Instrument Development Laboratories Inc.) which has a bandpass at 0.65 μ. Both pyrometers were calibrated to 3400°K by means of a standard lamp whose filament temperature was measured with a conventional disappearing-filament type optical pyrometer (Pyrometer Instrument Co. Inc.). The calibration of this latter pyrometer is traceable to the National Bureau of Standards. The motion pictures were taken with a 16 mm camera at a framing rate of 24 frames per sec, and the film was analyzed by means of a film reader to determine surface recession and shape change as a function of time.

Ablation Specimen

For these tests, a representative fine-grain graphite was selected as a standard grade against which other grades of artificial graphite and other graphitic materials can be compared in the future. The grade selected was ATJ which has a density of 1.73 g/cm and is produced by Union Carbide Corp. It is described, and some of its properties given, in Ref. 12. This grade was selected because it has been flight tested, and there is a considerable body of data available on its thermophysical and ablative properties. The material was procured in large billets measuring 51 cm by 61 cm by 23 cm thick. In all cases, the specimens were cut with their centerline parallel to the 23 cm billet dimension, the direction in which pressure is applied during the molding process. Thus the specimen centerline is in the "across grain" direction.[13]

The design of the ablation specimen evolved as the program progressed. Initial tests were made with hemisphere-cylinder specimens of either 1.52 cm diam or 3.04 cm diam as shown in Fig. 2a. As test conditions became more severe, however, it became apparent that there was significant shape change occurring during a run, the specimens becoming more blunt. In an

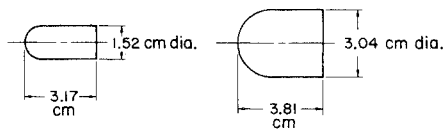

a) Hemispherical shapes.

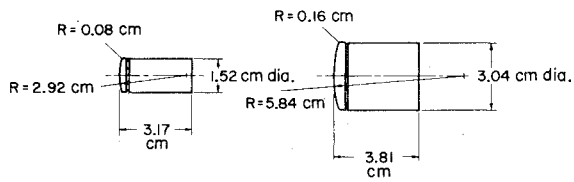

b) Blunt shapes.

Fig. 2 Ablation specimens.

attempt to determine a stable shape, tests were performed with 1.52 cm diam flat face specimens in several of the more severe environments, and the blunt shape§ shown in Fig. 2b was derived. The rest of the tests were then performed with this shape which was scaled up for the 3.04 cm diam specimens. Post run measurements show that the shape sometimes varied from that shown in Fig. 2b, but this was not too significant in terms of effective nose radius. The effects of nose radius will be discussed later when data for blunt and initially hemispherical specimens are compared.

Description of Tests and Measurements

The experimental techniques employed in the present tests are similar to those of earlier work.[14] At moderate test conditions, the surface recession rate V_s was determined by inserting three or four ablation specimens into the stream for increasing exposure times. The minimum exposure time was large compared to the duration of the initial transient, so the recession-time histories are linear. Thus V_s is simply the slope of the linear recession curve, and the experimental mass-loss rate, $\dot{m}_e$, is obtained by multiplying V_s by the bulk density. Under most of the more severe test conditions, a single ablation specimen was exposed to the stream, and the surface recession rate was determined from the motion pictures. During analysis of the earlier films, it became apparent that there is measurable thermal expansion of the ablation specimen, as well as the sting and support arm. Such expansion effects tend to reduce the apparent value of V_s as determined from the films. To avoid this problem, a notch was cut near the nose of the blunt ablation specimens (Fig. 2b) to provide a local reference for the recession measurements.

Stream survey results for a moderate test condition are shown in Fig. 3a where the measured values of heating rate and pressure have been normalized by their corresponding centerline values. This particular run was made with the N4001 arc heater coupled to the 8.6 cm diam conical nozzle, and the stagnation point pressure was 1.05 atm. Note that the heating rate and pressure profiles are flat to within 10% to a radius of about 1.5 cm and 3 cm, respectively.

Heat-transfer results obtained with six slug-type calorimeters during the same run are shown in Fig. 3b. The results are plotted in the form of heat-transfer rate vs nose radius, and a curve which relates heat-transfer rate to $R_n^{-1/2}$ has been faired through the result for one of the hemispherical calorimeters. Note that the results from all five hemispherical calorimeters lie within 8% of the curve, and that the results for the two 3.04 cm diam hemispherical calorimeters agree with 5%. The result for the 1.52 cm diam blunt calorimeter is plotted at an effective nose radius which was calculated by the method of Zoby and Sullivan.[15]

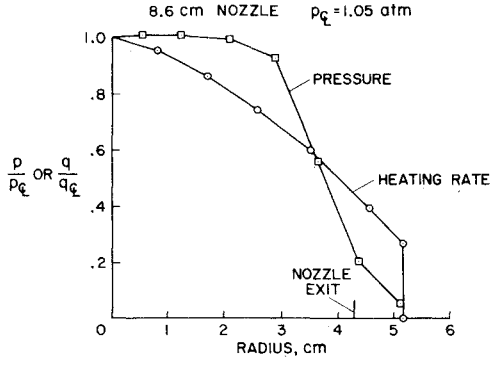

Fig. 3a Experimental results: results of stream surveys.

§ A few runs were also made with a shape somewhat less blunt than that shown in Fig. 2b. These specimens were 1.52 cm in diam and had a nose radius of 1.98 cm.

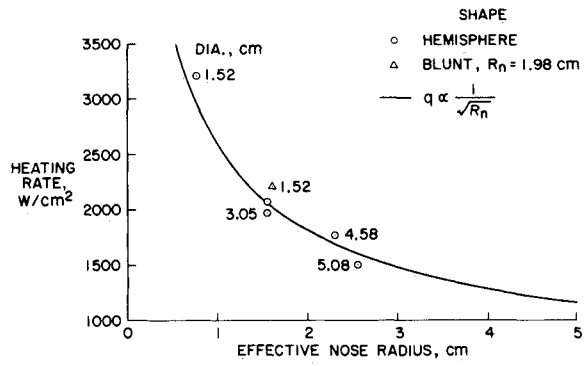

Fig. 3b Experimental results: heating rate results.

Heat-transfer results comparable to those shown in Fig. 3 were obtained during most of the tests in the 8.6 cm diam nozzle and during the lower current, lower pressure runs in the 5.5 cm diam conical nozzle. These results confirmed that the method of Zoby and Sullivan is adequate to predict the effective nose radius for the blunt configurations. Thus for all runs, this method was used to determine an effective nose radius from the measured post-test nose radius of the ablation specimen.

It will be shown later that surface temperature is a very critical measurement and therefore warrants some discussion. Measurements at more than one wavelength were made in an attempt to see if there were possible temperature errors due to radiation from the gas cap in front of the specimen. In virtually all cases where there was not an obvious problem, the two pyrometers agreed to within about 1%, and neither pyrometer consistently read higher than the other pyrometer. This result is a strong indication that gas cap emission was not a problem during the present tests. A further check of this potential problem was made by performing several tests where one of the pyrometers was removed and a Cary 14 spectrophotometer was set up to view the specimen surface through the pyrometer window. In all these tests, at a variety of surface temperatures, only continuum radiation and no line radiation was measured. This again indicates that gas cap emission was not a problem, and the result is compatible with theoretical calculations by Rindal et al.[16] These temperature measurements are brightness temperatures which must be converted to true temperatures by making an emissivity correction. This correction is at most an increase of about 70°K because the emissivity of graphite is relatively high. Emissivity values of 0.92 at a wavelength of 0.65 μ and 0.91 at a wavelength of 0.80 μ were selected from the work of Wilson and Spitzer.[17]

Thermochemical Ablation Theory

The term thermochemical implies that the theories to be discussed consider only mass removal by chemical reactions or sublimation. To date, no complete theory for mass removal by mechanical erosion exists.

There are basically two types of graphite ablation theories, the more rigorous solutions represented by Ref. 18 where boundary-layer transport phenomena are treated in detail without the simplifying assumptions of unity Lewis number and equal diffusion coefficients, and the approximate but more general theories[3-5] where the boundary-layer phenomena are treated in a gross manner by means of transfer coefficients and the assumptions of unity Lewis number and equal diffusion coefficients are made. It should be noted that other approximate theories exist which treat the more general case of a charring ablator, and these of course can be applied to graphite ablation. Of this group, the theory and computer code described in Ref. 19 has been used in the present program to calculate the thermochemical ablation of graphite based on the species and properties

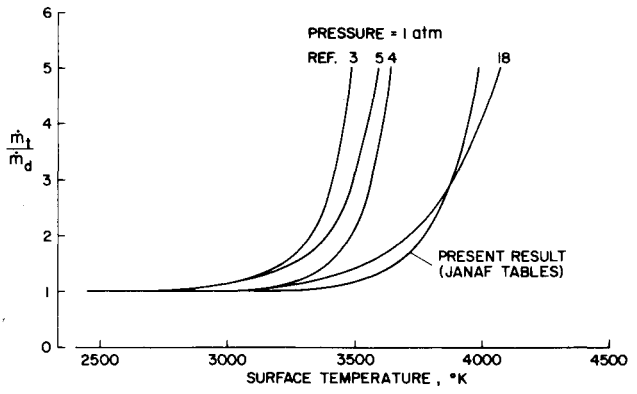

Fig. 4 Thermochemical ablation of graphite.

given in the JANAF tables,[2] and the results of these calculations will be presented later. The validity of the approximate theories can be ascertained by comparing them with the more rigorous theories. This has been done in Ref. 3 where it is shown that the approximate theory agrees quite well with the more rigorous theory[18] when the same species and properties are used in both cases. The approximate theories all use similar analytical techniques and differ basically only in the species included in the analysis and in the thermodynamic properties assigned to the species. A description of the differences in species and properties used in the several graphite ablation theories (rigorous as well as approximate) is beyond the scope of this paper, and the reader is referred to Ref. 6 for such a description.

The important point is that the different sets of species and properties do result in a very significant disparity in the thermochemical ablative performance of graphite as predicted by the various theories. This fact was noted in the Introduction and is graphically illustrated in Fig. 4 where the ratio¶ of the thermochemical mass-loss rate ($\dot{m}_t$) to the mass-loss rate for diffusion-controlled oxidation ($\dot{m}_d$) is plotted as a function of surface temperature. Here the results from the various theories, each incorporating a different set of species and properties, are plotted for a surface pressure of 1 atm. A similar disparity exists at all pressures, and so it is apparent that the selection of chemical species and thermodynamic properties does have a marked effect on the theoretical thermochemical ablation of graphite.

In order to determine which set of species and properties is valid, let us now discuss the experimental results of the present investigation and then compare the results with the various theories.

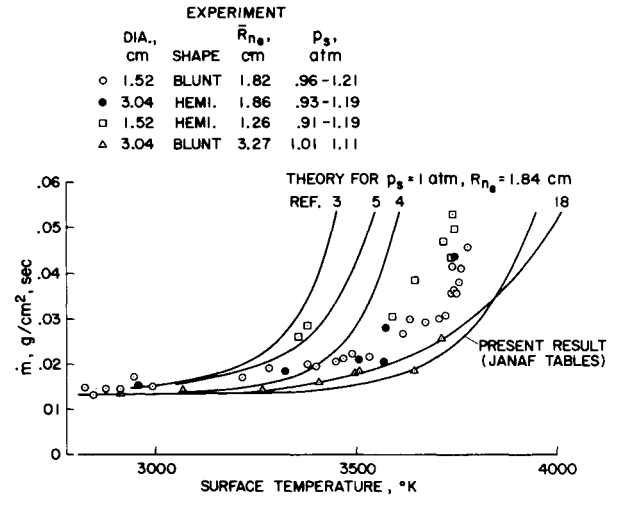

Fig. 5 Comparison of experiment and theory for a nominal pressure of 1.0 atm.

Results and Discussion

Experimental results similar to those described previously have been obtained over the following ranges of test conditions; $p_s = 0.30$ to 4.4 atm, q_c** = 815 to 8150 w/cm², $R_{n_e} = 0.85$ to 3.72 cm. Over these ranges of conditions, the measured surface recession rate varied from 0.00478 to 0.120 cm/sec, the mass-loss rate varied from 0.00827 to 0.208 g/cm² sec, and the surface temperature varied from 2570° to 4030°K. The experimental results obtained under the above ranges of test conditions are given in Table 1.

From the foregoing ranges of conditions, a surface pressure of 1 atm and the 1.52 cm diam blunt specimen with an initial nose radius of 2.92 cm were selected as the "standard" conditions for which most of the data were obtained. Additional data were obtained at other values of pressure and nose radius, so that at least the qualitative effects of these parameters on the experimental mass-loss rate could be determined.

Experimental Results for 1 atm Pressure

The results of the tests at a nominal surface pressure of 1 atm are shown in Fig. 5 where the mass-loss rate is plotted as a function of surface temperature. On the figure, the circular symbols†† represent results for a mean effective nose radius of about 1.84 cm, and the solid curves are theoretical results for the same nose radius. As noted previously, the curve labeled "present results" was obtained using the computer code described in Ref. 19 and the thermodynamic properties from the early JANAF tables. The experimental results are in reasonable agreement with the theories at the lower temperatures where the only removal mechanism is diffusion-controlled oxidation. But at higher temperatures, the experimental results fall between the approximate theory based on the JANAF tables and the other approximate theories. From this comparison we can conclude that the approximate theories of Refs. 3, 4, and 5, and the corresponding sets of species and properties on which they are based, are not valid because the measured surface temperatures are too high.

The remaining two theories are those of Scala and Gilbert[18] and the approximate theory based on the JANAF tables. At present, the theory of Scala and Gilbert is generally considered to be inaccurate because it does not include all the significant species.[5,6] Thus it is concluded that all the theories except the approximate theory based on the JANAF tables are invalid.‡‡ The disparity between this theory and the experimental results will be discussed later.

An interesting comparison between different specimen sizes and shapes is shown in Fig. 5. The filled symbols represent data obtained with 3.04 cm diam specimens which were initially hemispherical in shape. These specimens start with a nose radius of 1.52 cm; but, as mentioned previously, they tend to become more blunt with increasing exposure time. For these specimens,

¶ Generally the approximate theories calculate the mass-loss rate in terms of the parameter $B' = \dot{m}_v/\rho_e u_e C_H$ where $\rho_e u_e C_H$ is the transfer coefficient for stagnation point convective heat transfer in the presence of blowing. These results can be converted to the form shown in Fig. 4 by means of the relationship $\dot{m}/\dot{m}_d = (B'/B_d')(C_H/C_{H_d})$ where the subscript d refers to the diffusion-controlled oxidation regime. This conversion requires the assumption of a blowing relationship $C_H/C_{H_0} = f(B')$ where C_{H_0} is the Stanton number in the absence of blowing. The present calculations based on the JANAF tables were converted using the relationships $C_H/C_{H_0} = \ln(1.28B'+1)/1.28B'$ and $\rho_e u_e C_{H_0} = 113(p_s/R_{n_e})^{1/2}$ w kg/cm² MJ. The comparable relationships used in Refs. 3 and 4 are not specified.

** The convective heating rates listed are for a 1.52 cm diam hemispherical calorimeter.

†† Experimental results represented by the other symbols will be discussed later.

‡‡ This conclusion is based on comparison with equilibrium thermochemical ablation theories. We cannot, however, rule out the possibility that the sublimation process is rate controlled.[3]

Table 1 Experimental results

a) 1.52-cm-diameter hemisphere specimens

p_s, atm	T_s, K	R_{n_i}, cm	R_{n_f}, cm	R_{n_e}, cm	V_s, cm/sec	$\dot{m}_e$, g/cm²sec	$\dot{m}_t$, g/cm²sec	$\Delta\dot{m}$ g/cm²sec
.91	3356	.762	.864	.858	.0151	.0262	.0200	.0062
.93	3378	.762	.953	.939	.0167	.0288	.0196	.0092
.97	3739	.762	1.524	1.361	.0251	.0435	.0283	.0152
1.03	3739	.762	1.651	1.417	.0310	.0532	.0276	.0256
1.04	3744	.762	1.270	1.193	.0290	.0501	.0307	.0194
1.05	3589	.762	1.143	1.104	.0178	.0307	.0228	.0079
1.10	3717	.762	1.651	1.437	.0272	.0473	.0264	.0209
1.19	3644	.762	2.794	1.773	.0225	.0388	.0207	.0181
2.75	3894	.762	1.270	1.193	.0698	.121	.0502	.0708
2.85	3911	.762	1.270	1.193	.0673	.117	.0528	.0642
3.06	3894	.762	1.651	1.424	.0676	.117	.0467	.0703
3.28	3922	.762	1.270	1.193	.0815	.141	.0546	.0864
3.90	3947	.762	1.524	1.361	.0916	.159	.0556	.103
4.42	4033	.762	1.397	1.280	.120	.207	.0727	.134

b) 1.52-cm-diameter blunt specimens

p_s, atm	T_s, K	R_{n_i}, cm	R_{n_f}, cm	R_{n_e}, cm	V_s, cm/sec	$\dot{m}_e$, g/cm²sec	$\dot{m}_t$, g/cm²sec	$\Delta\dot{m}$ g/cm²sec
.49	2611	2.92	2.16	1.69	.00620	.0107	.00986	.00084
.50	2572	2.92	2.29	1.73	.00610	.0105	.00986	.00064
.50	3611	2.92	2.16	1.69	.0106	.0184	.0167	.0017
.51	3039	2.92	2.16	1.69	.00899	.0156	.0101	.0055
.53	2833	2.92	2.16	1.69	.00795	.0137	.0103	.0034
.59	3444	2.92	2.29	1.73	.0103	.0178	.0126	.0052
.60	3678	2.92	3.30	2.01	.0131	.0226	.0138	.0088
.96	2844	2.92	2.29	1.75	.00698	.0121	.0136	.0015
.97	2875	2.92	2.29	1.75	.00846	.0146	.0137	.0009
.97	3217	2.92	2.03	1.63	.0100	.0173	.0144	.0029
1.00	3447	2.92	2.16	1.66	.0121	.0209	.0159	.0050
1.00	3706	2.92	2.67	1.86	.0175	.0303	.0220	.0083
1.00	3756	2.92	2.79	1.90	.0221	.0383	.0250	.0133
1.00	3761	2.92	2.67	1.86	.0240	.0414	.0259	.0155
1.01	2822	2.92	2.03	1.63	.00868	.0150	.0145	.0005
1.01	2911	2.92	2.41	1.78	.00840	.0145	.0138	.0007
1.01	3283	2.92	2.54	1.81	.0112	.0193	.0141	.0052
1.01	3378	2.92	2.03	1.63	.0118	.0203	.0153	.0050
1.01	3617	2.92	3.43	1.98	.0156	.0270	.0177	.0093
1.01	3722	1.98	4.06	2.12	.0178	.0309	.0216	.0093
1.01	3739	1.98	2.92	1.92	.0208	.0360	.0237	.0123
1.03	3532	2.92	2.92	1.92	.0127	.0220	.0161	.0059
1.04	2992	2.92	2.16	1.69	.00878	.0152	.0145	.0007
1.04	3400	2.92	3.05	1.95	.0114	.0197	.0145	.0052
1.04	3672	2.92	2.92	1.92	.0170	.0294	.0203	.0091
1.04	3744	1.98	2.29	1.75	.0211	.0365	.0253	.0112
1.04	3750	2.92	2.79	1.89	.0206	.0357	.0247	.0110
1.07	2944	2.92	1.91	1.57	.00995	.0172	.0151	.0021
1.07	3489	2.92	2.16	1.69	.0131	.0226	.0165	.0061
1.07	3739	2.92	3.68	2.06	.0241	.0417	.0231	.0186
1.09	3467	2.92	2.03	1.62	.0124	.0215	.0169	.0046
1.10	3100	2.92	1.78	1.52	.0113	.0195	.0156	.0039
1.11	3633	2.92	2.79	1.89	.0174	.0302	.0192	.0110
1.21	3778	2.92	2.92	1.92	.0264	.0459	.0269	.0190
1.53	3778	1.98	2.16	1.69	.0300	.0518	.0294	.0224
1.57	3706	2.92	2.54	1.80	.0234	.0406	.0277	.0129
2.02	3828	2.92	1.65	1.42	.0498	.0859	.0376	.0483

b) Concluded

p_s, atm	T_s, K	R_{n_i}, cm	R_{n_f}, cm	R_{n_e}, cm	V_s, cm/sec	$\dot{m}_e$, g/cm²sec	$\dot{m}_t$, g/cm²sec	$\Delta\dot{m}$ g/cm²sec
2.03	3311	2.92	1.78	1.52	.0127	.0219	.0215	.0004
2.10	3744	2.92	2.29	1.73	.0236	.0408	.0288	.0120
2.10	3839	2.92	2.16	1.69	.0472	.0815	.0357	.0458
2.10	3856	2.92	2.41	1.78	.0452	.0781	.0363	.0418
2.10	3756	2.92	2.92	1.92	.0234	.0404	.0278	.0126
2.13	3811	2.92	3.43	2.03	.0361	.0625	.0306	.0319
2.17	3700	2.92	3.43	2.03	.0231	.0400	.0251	.0149
2.21	3844	2.92	2.67	1.86	.0424	.0732	.0347	.0385
2.23	3744	2.92	2.92	1.92	.0302	.0522	.0278	.0244
2.31	2889	2.92	1.91	1.57	.0112	.0193	.0222	.0029
2.58	3700	2.92	3.05	1.96	.0222	.0384	.0266	.0118
2.87	3578	2.92	1.78	1.52	.0229	.0397	.0282	.0115
2.91	3739	2.92	1.65	1.42	.0267	.0460	.0343	.0117
2.92	3644	2.92	1.91	1.57	.0240	.0415	.0298	.0117
3.06	3894	2.92	2.48	1.79	.0666	.115	.0416	.0734
3.11	3789	2.92	3.05	1.96	.0376	.0650	.0324	.0326
3.21	3917	2.92	1.91	1.57	.0668	.116	.0470	.0690
3.24	3828	2.92	2.16	1.69	.0510	.0884	.0377	.0507
3.41	3908	2.92	1.82	1.57	.0678	.117	.0467	.0703
3.63	3889	2.92	2.41	1.78	.0683	.118	.0424	.0756
4.04	3856	2.92	2.41	1.78	.0589	.102	.0406	.0614
4.14	3378	2.92	1.52	1.36	.0194	.0335	.0329	.0006
4.23	3956	2.92	2.29	1.73	.0980	.170	.0508	.119

c) 3.04-cm-diameter hemisphere specimens

p_s, atm	T_s, K	R_{n_i}, cm	R_{n_f}, cm	R_{n_e}, cm	V_s, cm/sec	$\dot{m}_e$, g/cm²sec	$\dot{m}_t$, g/cm²sec	$\Delta\dot{m}$ g/cm²sec
.31	2728	1.52	1.65	1.65	.00478	.00825	.00796	.00029
.32	3317	1.52	1.78	1.76	.00526	.00908	.00884	.00025
.93	3322	1.52	1.78	1.76	.0107	.0185	.0139	.0046
.96	3567	1.52	1.91	1.88	.0121	.0209	.0165	.0044
.97	3722	1.52	2.29	2.20	.0193	.0335	.0211	.0124
1.04	3706	1.52	2.29	2.21	.0218	.0378	.0204	.0174
1.05	3506	1.52	1.91	1.88	.0123	.0214	.0160	.0054
1.14	2956	1.52	1.78	1.76	.00800	.0139	.0147	.0008
1.17	3744	1.52	2.16	2.10	.0254	.0439	.0235	.0204
1.19	3572	1.52	1.78	1.76	.0147	.0255	.0185	.0070
1.37	3194	1.52	1.78	1.76	.0122	.0211	.0162	.0049
1.94	3294	1.52	1.88	1.85	.0137	.0236	.0190	.0046
2.42	3028	1.52	1.78	1.76	.0118	.0204	.0214	.0010

d) 3.04-cm-diameter blunt specimens

p_s, atm	T_s, K	R_{n_i}, cm	R_{n_f}, cm	R_{n_e}, cm	V_s, cm/sec	$\dot{m}_e$, g/cm²sec	$\dot{m}_t$, g/cm²sec	$\Delta\dot{m}$ g/cm²sec
.50	2756	5.84	4.77	3.56	.00691	.0119	.00688	.0050
.50	3511	5.84	5.08	3.63	.00828	.0143	.00908	.0052
.50	3578	5.84	4.77	3.56	.00904	.0157	.0105	.0052
.50	3611	5.84	3.81	3.18	.00823	.0143	.0122	.0021
.57	3389	5.84	5.40	3.72	.00856	.0148	.0081	.0067
1.01	2911	5.84	3.51	3.00	.00808	.0140	.0106	.0034
1.04	3067	5.84	3.51	3.00	.00833	.0144	.0108	.0036
1.04	3494	5.84	4.45	3.46	.0106	.0184	.0115	.0069
1.07	3406	5.84	4.76	3.55	.00940	.0163	.0108	.0055
1.10	3100	5.84	3.30	2.87	.00841	.0145	.0117	.0028
1.10	3506	5.84	4.45	3.46	.0107	.0186	.0121	.0065
1.10	3644	5.84	3.81	3.18	.0108	.0187	.0151	.0036
1.11	3711	5.84	5.08	3.63	.0152	.0263	.0164	.0099

the actual nose radius was measured at the end of the exposure and the effective nose radius was determined. Only runs where the effective nose radius falls within the range obtained with the 1.52 cm diam blunt models are included in Fig. 5. It is apparent that the results obtained with the specimens of two different sizes and shapes are in agreement. Thus reliable results can be obtained with hemispherical specimens if the shape change is accounted for.

Having established this fact, let us discuss results obtained with 1.52 cm diam hemispherical specimens. A few data points obtained with this specimen shape are included in Fig. 5. For these points, the mean effective nose radius is 1.26 cm, compared to 1.82 cm for the 1.52 cm diam blunt specimens. As we would expect from theoretical considerations, the smaller nose radius does lead to higher mass-loss rates.

Also shown in Fig. 5 are a few data points obtained with 3.04 cm diam blunt specimens at a nominal pressure of 1 atm. At high temperatures, these results fall below those obtained with the 1.52 cm diam specimens as we would again expect from theoretical considerations. At lower temperatures, however, the results obtained with the two different size specimens are almost comparable. The exact reason for this is not known.

Experimental Results at Other Pressures

Experimental results, obtained at pressures other than 1 atm, are shown in Fig. 6 where the results for 1 atm are reproduced for comparison. All results shown on this figure are for a mean effective nose radius of 1.80 cm, and the solid curves represent theoretical results, based on the JANAF tables, for this same nose radius. As noted previously, the experimental and theoretical

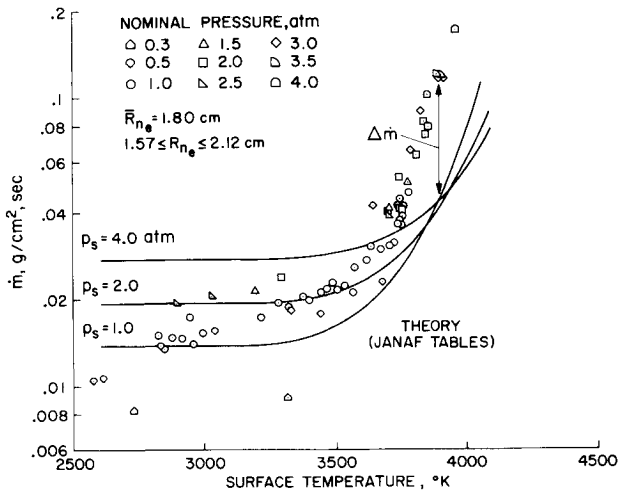

Fig. 6 Comparison of experiment and theory.

results are generally in good agreement at lower temperatures but not at the higher temperatures. In fact, at 4000°K the experimental results lie above the theory by a factor of three.

The disparity between the experimental and theoretical results can be illustrated more graphically by correlating the incremental mass-loss rate which is defined as $\Delta\dot{m} = \dot{m}_e - \dot{m}_t$. In this expression, $\dot{m}_t$ is the corresponding theoretical mass-loss rate which is determined using the experimental values of surface temperature, pressure and effective nose radius. Both $\Delta\dot{m}$ and $\dot{m}_t$ are tabulated in Table 1.

The incremental mass-loss rate correlates with surface temperature as shown in Fig. 7. All the experimental results of the present tests at pressures from 0.3 to 4.4 atm and effective nose radii from 0.85 to 3.72 cm are included in the correlation, where different nominal values of pressure are denoted by different symbols. It is apparent that $\Delta\dot{m}$ does not correlate with either pressure or nose radius but depends solely upon surface temperature. It increases from almost zero at 3000°K to 0.13 g/cm²sec at 4000°K. Thus at the higher temperature $\Delta\dot{m}$ is about twice the value of $\dot{m}_t$.

The pressure independence of $\Delta\dot{m}$ results from the fact that the total measured mass-loss rate, $\dot{m}_e$, becomes independent of pressure at high temperatures. This is evident in Fig. 6 where, at temperatures above about 3700°K, $\dot{m}_e$ increases exponentially with temperature. It doubles for an increase in temperature of about 110°K. In the same temperature range, the theoretical curves are crossing so the effect of pressure on $\dot{m}_t$ is minimal. The net result is that $\Delta\dot{m}$ is essentially independent of pressure.

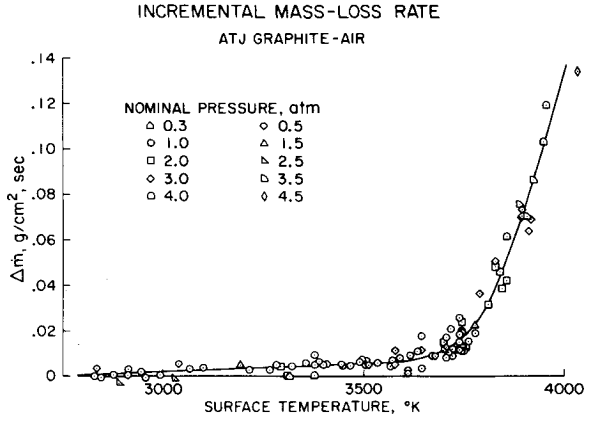

Fig. 7 Incremental mass-loss rate.

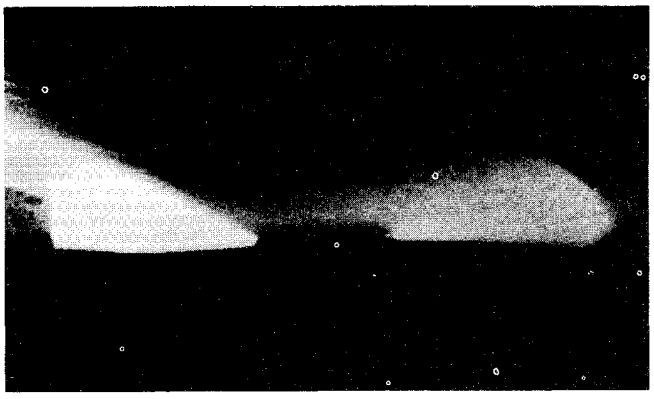

Fig. 8 Particulate mass loss (specimen stagnation point on the right side).

Particulate Mass Loss

At least part of the disparity between experiment and theory can be attributed to particulate mass loss. In all tests at surface temperatures above about 3000°K, a shower of small particles can be seen in the flow downstream of the ablating specimen, the shower being more profuse at higher temperatures. An interesting point is that the particles do not show up in the motion pictures of the ablating specimen. This is believed to be the result of large luminosity differences between a minute particle and the much larger specimen. In order to circumvent this problem, a run was made with a sheet metal plate placed about 30 cm from the nozzle centerline and at a height such that its top was in line with the top surface of the specimen during exposure to the stream. The purpose, of course, was to block out the intensely luminous specimen but not the particles coming off its upper surface. An enlargement of one frame of the motion picture obtained during this run is shown in Fig. 8 where a myriad of particle tracks are visible. Part of the specimen surface is also visible due to diametral expansion and diffraction.

At present, the nature of the mechanism for particulate mass loss is the subject of much debate. One proposed model[4,20] for the mechanism is based on the fact that, on a microscale, graphite is a very heterogeneous material[13] composed of two constituents—filler particles held together by a binder matrix. These two constituents may differ markedly in such properties as density, porosity, degree of graphitization, chemical reactivity, and vaporization characteristics. The model hypothesizes that differences in one or more of these properties lead to preferential erosion of the binder, leaving the filler particles unsupported and susceptible to removal by aerodynamic forces. Another possible cause for particulate mass loss, which has been suggested by the present authors,[21] is thermal stress. Whatever its cause, the occurrence of particulate mass loss is detrimental because it indicates that graphite does not realize its full thermochemical potential for accommodating heat.

The work described previously demonstrates that particulate mass loss does occur at low pressures and thus is not a problem unique to high-pressure ballistic missile environments. At present, the magnitude of the particulate mass-loss rate is unknown. Whether all or only a fraction of $\Delta\dot{m}$ is the result of particulate mass loss cannot be determined from the present test results. Further tests must be performed to measure the particulate mass-loss rate directly. Once this rate is known, it can be deducted from the total mass-loss rate to determine the actual thermochemical mass-loss rate.

Summary and Conclusions

An experimental investigation has been performed to determine the ablative behavior of ATJ graphite in an air stream. In these tests the surface pressure varied from 0.3 to 4.4 atm,

the effective nose radius varied from 0.85 to 3.72 cm, and the surface temperature varied from 2570° to 4030°K. From the test results it is concluded that: 1) All the approximate equilibrium thermochemical ablation theories, except the one based on the thermodynamic properties from the JANAF tables, are invalid because they overpredict the mass-loss rate. 2) The theory based on the JANAF properties is in good agreement with the experimental results in the diffusion-controlled oxidation regime but underpredicts the experimental mass-loss rate at higher temperatures. At 4000°K, for example, the experimental rate is a factor of three greater than the theoretical rate. 3) At temperatures above 3700°K, the experimental mass-loss rate becomes independent of pressure and an exponential function of temperature; it doubles for an increase in temperature of about 110°K. 4) At least a portion of the disparity between the experimental and theoretical mass-loss rates is due to particulate mass loss which is visually observed at temperatures above about 3000°K.

The exact mechanism of particulate mass loss is uncertain at present. Determination of the details of this mechanism will require further experimental work on different grades of graphite with different constituents and microstructures, as well as a direct measure of the particulate mass-loss rate. Once the details of the mechanism are established, it may be possible to produce new grades of graphite which are less susceptible to particulate mass loss and therefore capable of realizing the full thermochemical potential of graphite as a heat shield material.

References

[1] Tauber, M. E. and Wakefield, R. M., "Heating Environment and Protection During Jupiter Entry," *Journal of Spacecraft and Rockets*, Vol. 8, No. 6, June 1971, pp. 630–636.

[2] *JANAF Thermochemical Tables* (and Supplements to 1966), The Dow Co., Midland, Mich.

[3] Dolton, T. A., Goldstein, H. E., and Maurer, R. E., "Thermodynamic Performance of Carbon in Hyperthermal Environments," *AIAA Progress in Astronautics and Aeronautics Thermal Design Principles of Spacecraft and Entry Bodies*, Vol. 21, edited by J. T. Bevans, Academic Press, New York, 1969, pp. 169–201.

[4] Kratsch, K. M., Martinez, M. R., Clayton, F. I., Greene, R. B., and Wuerer, J. E., "Graphite Ablation in High Pressure Environments," AIAA Paper 68-1153, Williamsburg, Va, 1968.

[5] Fogaroli, R. P. and Brant, D. N., "Re-evaluation of Graphite Thermochemical Ablation," TFM-9151-060, Oct. 1968, Thermodynamics Lab., Re-entry Systems Dept., General Electric Co., Philadelphia, Pa.

[6] Rindal, R. A. and Powars, C. A., "Effects of Carbon Vapor Thermochemistry Uncertainties on R/V Ablation Predictions," AIAA Paper 71-414, Tullahoma, Tenn., 1971.

[7] Metzger, J. W., Engel, M. J., and Diaconis, N. S., "Oxidation and Sublimation of Graphite in Simulated Re-entry Environments," *AIAA Journal*, Vol. 5, No. 3, March 1967, pp. 451–460.

[8] Bishop, W. N. and DiCristina, V., "The Combustion and Sublimation of Carbon at Elevated Temperatures," AIAA Paper 68-759, Los Angeles, Calif., 1968.

[9] Tanzilli, R. A., "Evaluation of Graphite Composites in Re-entry Environments," AFML TR 65-328, Oct. 1965, Air Force Materials Lab., Wright-Patterson Air Force Base, Ohio.

[10] Miller, I. M. and Sutton, K., "An Experimental Study of the Oxidation of Graphite in High Temperature Supersonic and Hypersonic Environments," TN D-3444, 1966, NASA.

[11] Maahs, H. G. and Schryer, D. R., "Particle Removal in the Ablation of Artificial Graphite," *AIAA Journal*, Vol. 7, No. 11, Nov. 1969, pp. 2178–2179.

[12] *The Industrial Graphite Engineering Handbook*, Carbon Products Div., Union Carbide Corp., New York.

[13] Riley, W. C., "Graphite," *High Temperature Materials and Technology*, edited by I. E. Campbell and E. M. Sherwood, Wiley, New York, 1967.

[14] Lundell, J. H., Dickey, R. R., and Jones, J. W., "Performance of Charring Ablative Materials in the Diffusion-Controlled Surface Combustion Regime," *AIAA Journal*, Vol. 6, No. 6, June 1968, pp. 1118–1126.

[15] Zoby, E. V. and Sullivan, E. M., "Effects of Corner Radius on Stagnation Point Velocity Gradients on Blunt Axisymmetric Bodies," TM X-1067, March 1965, NASA.

[16] Rindal, R. A., Kennedy, W. S., Powars, C. A., and Baker, D. L., "High Pressure Ablation Characterization of Graphite for Nose Tip Applications," *Graphitic Materials for Advanced Re-entry Vehicles*, edited by D. M. Forney, AFML TR 70-133, Pt. 1, Aug. 1970, Air Force Materials Lab., Wright-Patterson Air Force Base, Ohio.

[17] Wilson, R. G. and Spitzer, C. R., "Visible and Near-Infrared Emittance of Ablation Chars and Carbon," *AIAA Journal*, Vol. 6, No. 4, April 1968, pp. 665–671.

[18] Scala, S. M. and Gilbert, L. M., "Sublimation of Graphite at Hypersonic Speeds," *AIAA Journal*, Vol. 3, No. 9, Sept. 1965, pp. 1635–1644.

[19] McCuen, P. A. et al., "A Study of Solid Propellant Rocket Motor Exposed Materials Behavior," Final Rept., Contract AF 04(611)-9073, Feb. 1965, Vidya Div., Itek Corp., Palo Alto, Calif.

[20] McVey, D. F., Auerbach, I., and McBride, D. D., "Some Observations on the Influence of Graphite Microstructure on Ablation Performance," AIAA Paper 70-155, New York, 1970.

[21] Lundell, J. H. and Dickey, R. R., "The Ablation of Graphitic Materials in the Sublimation Regime," AIAA Paper 72-298, Tullahoma, Tenn., 1972.